

## Analytical and Numerical Study of Three Main Migration Laws for Vesicles Under Flow

Alexander Farutin\* and Chaouqi Misbah†

Laboratoire Interdisciplinaire de Physique/UMR5588, Université Grenoble I/CNRS, Grenoble F-38041, France

(Received 18 July 2012; published 6 March 2013)

Blood flow shows nontrivial spatiotemporal organization of the suspended entities under the action of a complex cross-streamline migration, that renders understanding of blood circulation and blood processing in lab-on-chip technologies a challenging issue. Cross-streamline migration has three main sources: (i) hydrodynamic lift force due to walls, (ii) gradients of the shear rate (as in Poiseuille flow), and (iii) hydrodynamic interactions among cells. We derive analytically these three laws of migration for a vesicle (a model for an erythrocyte) showing good agreement with numerical simulations and experiments. In an unbounded Poiseuille flow, the situation turns out to be quite complex. We predict that a vesicle may migrate either towards the center or away from it, or even show both behaviors for the same parameters, depending on initial position. This finding can both help understanding healthy and pathological erythrocyte behavior in blood circulation and be exploited in biotechnologies for cell sorting out.

DOI: [10.1103/PhysRevLett.110.108104](https://doi.org/10.1103/PhysRevLett.110.108104)

PACS numbers: 87.16.D-, 47.15.G-, 47.60.Dx, 87.19.U-

*Introduction.*—Cross-streamline migration under flow plays a major role in suspensions of soft matter and biology, where inertia of the suspended entities is often small (the Stokes regime). Typical examples include, among others, emulsions, DNA solutions, vesicle and capsule suspensions, and blood. Cross-streamline migration also plays a decisive role in several industrial and medical applications, such as polymer processing [1], DNA sorting [2], and hemodynamics [3], to name but a few. A prominent example in blood flow is the lateral motion of erythrocytes towards the flow centerline resulting in a drastic reduction of blood flow resistance in the microvasculature (Fåhræus-Lindqvist effect). Cell migration properties can be exploited in lab-on-chip technologies in order to perform biofluid separation, medical diagnosis, and so on.

The general picture is that the suspended entities in these types of solutions (e.g., red blood cells —RBCs— in blood) exhibit cross-streamline displacement, provided that the symmetry of the Stokes flow is broken. For example, the time reversal symmetry of the Stokes equations precludes this type of migration for solid spherical particles. Contrariwise, the ability of soft suspended entities to deform in response to flow stresses may lead to an upstream-downstream asymmetry resulting in the breakdown of the overall time reversal symmetry (Stokes equations combined with boundary conditions on the soft boundaries). The main situations leading to the breakdown of this symmetry are (i) shear flow close to a solid boundary, (ii) Poiseuille flow, and (iii) mutual interactions. As a result of the symmetry breaking, the suspended entities undergo cross-streamline migration. However, the migration direction, which follows from an interplay between particle elasticity and flow patterns, turns out to be a subtle phenomenon, as reported here.

Our study focuses on vesicles (a closed phospholipid membrane), which have known a tremendous upsurge of

interest in recent years [4], owing, in particular, to similarities with RBCs in their behavior under flow. Several steps forward have been undertaken regarding migration by experimental [5–8], analytical [9–13], and numerical studies [14–19], but a complete understanding of this phenomenon remains an issue due to the intrinsic complexity of the problem. For example, it was reported that a vesicle (or a RBC) placed away from the Poiseuille flow centerline should migrate towards the center [6,12,17,18]. We find here that the overall picture is far from being obvious: a vesicle can also migrate outwards until it reaches a wall, or stop at some intermediate position far away from the center, or stay off-centered but remain in the vicinity of the center, and so on.

*Problem formulation.*—The intrinsic properties of a vesicle can be characterized by the following parameters: The volume  $V = 4\pi R_0^3/3$ , where  $R_0$  is the radius of a sphere having the same volume, and the surface area  $A = 4\pi R_0^2(1 + \Gamma)$ , where the normed excess area from a sphere  $\Gamma$  is a dimensionless parameter measuring the degree of deflation of the vesicle. The volume and surface area of the vesicle are conserved due to the impermeability and inextensibility of the membrane. The viscosities of external and internal liquids are denoted as  $\eta_{\text{ext}}$  and  $\lambda\eta_{\text{ext}}$ , respectively, where  $\lambda$  is viscosity contrast. The membrane is endowed with the resistance to bending characterized by the bending modulus  $\kappa$ . The shear and Poiseuille flows are characterized by the shear rate  $\dot{\gamma}$  and the flow curvature  $\alpha$ , respectively:

$$v_x^\infty = \dot{\gamma}y, \quad v_x^\infty = \alpha(D^2/4 - y^2 - z^2) \quad (1)$$

in Cartesian coordinates  $(x, y, z)$ , where  $D$  is diameter of the tube (which is fictitious, because of assumption of unbounded flow; in a real system, we have in mind large  $D$  in comparison to cell diameter). In unbounded flow, one can add an arbitrary constant to the flow field

without affecting the physics; only the flow curvature  $\alpha$  matters. We define dimensionless capillary number as  $C_a = \dot{\gamma}R_0^3\eta_{\text{ext}}/\kappa$  [20] and  $C_a = \alpha R_0^4\eta_{\text{ext}}/\kappa$  [12] for shear and Poiseuille flows, respectively. For the analytical study, we consider typical values of  $\Gamma$  provided in the experimental literature, namely in the range 0 to 0.1 [5–8,21,22]. In most experimental studies [5,6,8], the flow strength is large as compared to bending forces, so that it is legitimate to consider the case where  $C_a \gg 1$ . This also holds in most sites of the microvasculature (since  $\dot{\gamma} \sim 10^2 - 8 \times 10^3 \text{ s}^{-1}$  [23]).

We focus formally on long-range asymptotic behavior for the pairwise interactions and the interaction with a wall, which allows for analytical tractability. Full numerical simulation will reveal, however, quantitative agreement with the analytical results even for distances of about two vesicle diameters. The full flow field can be represented as a sum of the imposed flow field  $\mathbf{v}_\infty$  and the disturbance flow  $\mathbf{v}$  induced by the vesicle. The induced flow at vector position  $\mathbf{R}$  (from vesicle) reads [24]

$$\mathbf{v}_i(\mathbf{R}) = -\frac{3}{8\pi} \frac{R_i R_j R_k S_{jk}}{\eta_{\text{ext}} R^5} + O(R^{-3}), \quad (2)$$

where repeated indices are to be summed over according to Einstein's convention and  $S_{ij}$  is a symmetric traceless tensor, called the stresslet of the particle. The Eq. (2) is valid if  $R \gg R_0$  and no external force acts on the vesicle. In this Letter, the analytical study (but not the numerical one) is concentrated on the situation where  $\lambda = 1$ , which offers a simplified expression for the stresslet:

$$S_{ij} = S'_{ij} - \frac{1}{3} \delta_{ij} S'_{kk}, \quad S'_{ij} = - \int r_i f_j dA, \quad (3)$$

where  $r_i$  is the membrane coordinate vector and  $f_j dA$  is the membrane force. This force is nothing but the bending one supplemented with the ‘‘tension’’ force associated with the Lagrange multiplier enforcing local inextensibility of the membrane [25]. The determination of the stresslet tensor  $S_{ij}$  is the key point in order to extract the analytical expressions of the migration laws. Our boundary integral simulations show that the bending part of the force attains a saturation as the capillary number is increased. Since the tension forces scale with the capillary number, it is legitimate to neglect the bending contribution of the force in favor of the tension one. Formally, this corresponds to setting  $C_a = \infty$ . Comparison between the numerical (obtained at finite, albeit large enough  $C_a$ ) and analytical results supports this statement (as shown below).

The evaluation of  $S_{ij}$  requires the determination of the vesicle shape and surface forces under flow. This can be achieved with the use of so-called small-deformation approximation [26] (which means small enough  $\Gamma$ ; unlike droplets, here, the maximal deformation is not set by  $C_a$  but by  $\Gamma$  due to membrane inextensibility). We expand the Stokes equations with boundary conditions in power series of  $\Gamma$  on the basis of spherical harmonics in a consistent

manner [27]. Here, we merely focus on the results and their consequences (see details in Ref. [28]).

*The three migration laws.*—(i) Wall-induced migration: The wall is located at  $y = 0$  [consistently with Ref. (1)] and  $y_0$  is the height of the centroid of the membrane above the wall. In general, given any physical entity (drop, vesicle, etc), the migration velocity can be expressed as [29]

$$V_m = -\frac{9}{64\pi\eta_{\text{ext}}} \frac{S_{yy}}{y_0^2} + O(y_0^{-3}). \quad (4)$$

The physical nature of the entity under consideration (e.g., vesicle) is carried by  $S_{ij}$ . In the long-range asymptotic regime, it is sufficient to use the shape and stresslet obtained in an unbounded shear flow. We first determine  $S_{yy}$  in powers series of  $\Gamma$ , which then yields for  $\lambda = 1$

$$V_m = \frac{69\dot{\gamma}R_0^3}{448y_0^2} \sqrt{30\Gamma} [1 - 2.360\Gamma + 19.05\Gamma^2 - 180.2\Gamma^3 + 1754.\Gamma^4 - 17021.\Gamma^5 + O(\Gamma^6)], \quad (5)$$

where we have converted fractions involving ratios of large natural numbers (given in Ref. [28]) into decimal numbers. For the sake of comparison with experiments [8], we determine two axes of the projection of the vesicle on the  $y = 0$  plane:  $\hat{a}_1$  ( $x$ -axis) and  $a_3$  ( $z$ -axis):

$$\hat{a}_1 = 2R_0 [1 + 6.473\Gamma - 18.69\Gamma^2 + 214.0\Gamma^3 - 3217.\Gamma^4 + 55346.\Gamma^5 - 995354.\Gamma^6 + O(\Gamma^7)], \quad (6)$$

$$a_3 = 2R_0 [1 - 2.321\Gamma + 9.120\Gamma^2 - 47.43\Gamma^3 + 248.1\Gamma^4 - 664.1\Gamma^5 - 12034.\Gamma^6 + O(\Gamma^7)]. \quad (7)$$

Our results are reported on Fig. 1 (solid line) in the plane of the the apparent asphericity  $\hat{a}_1/a_3$  and the dimensionless lift parameter  $\beta = 24V_m y_0^2 / (\dot{\gamma} \hat{a}_1 a_3^2)$ , as defined in experiments [8]. We performed numerical simulations

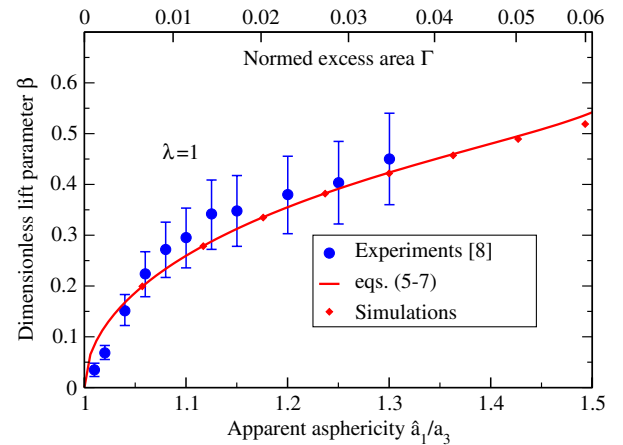


FIG. 1 (color online). Migration of a vesicle in a semibounded shear flow. Solid line corresponds to Eqs. (5)–(7). Small diamonds are results of boundary integral simulations with  $C_a = 100$ .

(small diamonds), using boundary integral method [30], to estimate the convergence of the expansion. Remarkable agreement is obtained between the present analytical theory, experiments and full numerical simulations. We find that Eq. (5) shows quantitative agreement with numerical simulations in wall-bounded shear flow even for distances as small as two vesicle diameters (see Discussion) and for  $\Gamma < 0.05$ . Note that the asymptotic behavior of  $V_m$  for almost spherical vesicles has been already calculated in Ref. [10] with an implied assumption  $\lambda = O(\Gamma^{-1/2})$ . Since we consider the case of  $\lambda = 1$ , it is not surprising that Eq. (5) shows different quantitative results from that in Ref. [10].

(ii) Migration in Poiseuille flow: Let us now consider the second source of migration, namely, the shear gradient in Poiseuille flow [Eq. (1)], which reveals an unexpected richness. Because the vesicle shape adapts itself rapidly to the imposed flow as compared to the migration time, the migration velocity solely depends on vesicle position. In general, this dependence is lengthy (see Ref. [28]), however, for  $y_0 \gg R_0$  [12], the velocity tends to a value that is independent of  $y_0$  (plateau on the right side in Fig. 2):

$$V_m = -\frac{\alpha R_0^2}{2} \sqrt{\frac{\Gamma}{30}} [1 - 10.019\Gamma + 104.92\Gamma^2 + O(\Gamma^3)] \quad (8)$$

with  $\lambda = 1$ . Equation (8) shows that not very deflated vesicles always migrate towards the center of a channel in strong flows (in agreement with the results in Ref. [12], where a planar Poiseuille flow was considered). Comparison with numerical simulations shows good agreement.

Exploring further the parameter space by means of a systematic numerical simulation (similar to that in Ref. [30], albeit with several improvements as described in Ref. [28]), we discover the existence of a new panel of scenarios. The complexity of the picture depends both on

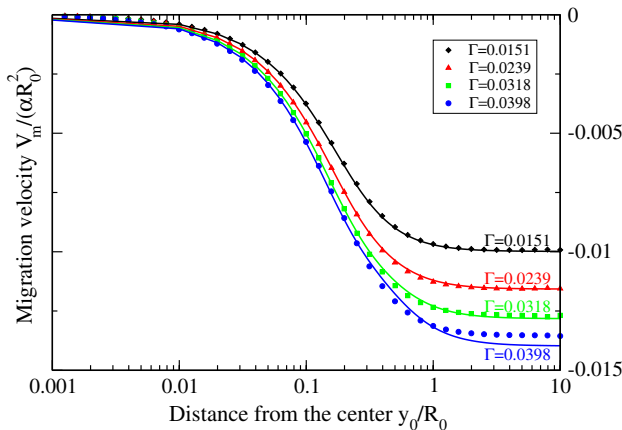


FIG. 2 (color online). Migration of a vesicle in unbounded Poiseuille flow. Solid lines are calculated analytically, symbols are the results of simulations using boundary integral method with  $C_a = 1000$ .

the capillary number  $C_a$  and the viscosity contrast  $\lambda$  (for a given  $\Gamma$ ). For  $\lambda = 1$  and  $\Gamma = 0.0728$ , we find that a vesicle initially placed away from the flow centerline always migrates towards the center for a high enough  $C_a$  (for example,  $C_a = 100$ ), and adopts an axisymmetric parachute shape. The same trend is observed for lower  $C_a$  ( $C_a = 25$ ), but we found that the final shape has a lower symmetry, a croissantlike shape [31]: instead of the full rotational symmetry around the centerline present in the parachute shape, the croissant enjoys only two orthogonal symmetry planes. In other words, by lowering  $C_a$ , we have a spontaneous symmetry-breaking bifurcation from parachute to croissant. Upon further decrease of  $C_a$  (down to  $C_a = 10$ ), we find that a vesicle migrates towards the center, approaches it, but never reaches it: the shape is a slipper [32–36]. For smaller values (the case  $C_a = 0.1$ ), the vesicle stops far from the center. Conversely, if the vesicle is placed at the flow centerline for  $C_a = 10$  and  $C_a = 0.1$ , it will either migrate slightly outwards (slipper for  $C_a = 10$ ) or significantly far away and stop ( $C_a = 0.1$ ) at some lateral position.

We have investigated further this question in the presence of a viscosity contrast ( $\lambda = 5$ , a typical value for RBCs). We have found that this ingredient completely destroys the above picture of migration. At large enough  $C_a$  ( $C_a = 1000$ ), with any initial position explored so far, we find an indefinite outward migration (i.e., without any tendency of stopping). For smaller values of  $C_a$ , the vesicle exhibits either a perpetual outward migration or stays in vicinity of the center (acquiring a slipper shape), depending on initial position. In other words, there is metastability. The basin of attraction of the slipper solution and its center of mass distance from the centerline increase as  $C_a$  is decreased. The various scenarios are summarized in Fig. 3.

(iii) Interaction between 2 vesicles: Finally, let us deal with the migration due to hydrodynamic interaction, which plays an essential role in so-called hydrodynamic diffusion. In order to characterize this phenomenon, we consider two identical vesicles in simple shear flow located in positions  $(x_0(t), y_0(t), 0)$  and  $(-x_0(t), -y_0(t), 0)$  and measure the difference in  $y$  components before and after the interaction:

$$\Delta y_i = 2 \lim_{t \rightarrow -\infty} y_0(t); \quad \Delta y_f = 2 \lim_{t \rightarrow \infty} y_0(t). \quad (9)$$

For  $\Delta y_i \gg R_0$ , Eq. (2) provides the disturbance of the flow due to hydrodynamic interactions, which yields the following differential equation for  $y_0(t)$ :

$$\dot{y}_0(t) = -\frac{3y_0(t)[S_{xx}x_0(t)^2 + 2S_{xy}y_0(t)x_0(t) + S_{yy}y_0(t)^2]}{32\pi\eta_{\text{ext}}[x_0(t)^2 + y_0(t)^2]^{5/2}}. \quad (10)$$

Because we are interested in the long-range interaction, we substitute the undisturbed dependence  $x_0(t) = \dot{\gamma}\Delta y_i t/2$ ,  $y_0(t) = \Delta y_i/2$  into the right hand side of Eq. (10).

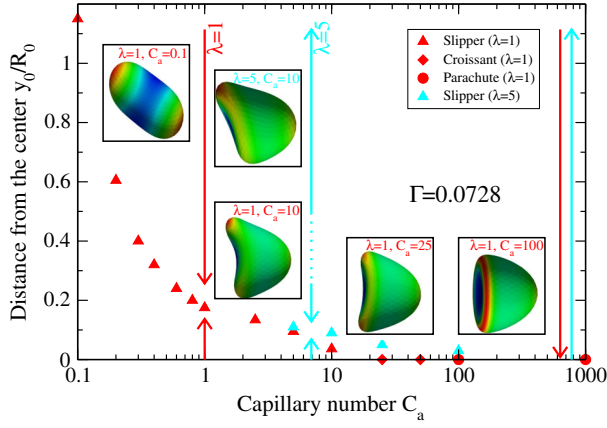


FIG. 3 (color online). Different scenarios of migration for  $\Gamma = 0.0728$  depending on  $C_a$  and  $\lambda$ . Results obtained from full numerical simulations. The symbols show stable terminal position (if any). The arrows indicate the direction of migration. The difference between slippers and croissants is evidenced by color code showing mean curvature. High-resolution images are provided in Ref. [28].

Then  $\Delta y_f - \Delta y_i$  can easily be obtained upon integration, yielding

$$\Delta y_f - \Delta y_i = -\frac{S_{xx} + 2S_{yy}}{2\pi\eta_{\text{ext}}\dot{\gamma}\Delta y_i^2} = \frac{S_{zz} - S_{yy}}{2\pi\eta_{\text{ext}}\dot{\gamma}\Delta y_i^2}. \quad (11)$$

Like Eq. (4), this expression is valid for any elastic particle. Using  $S_{ij}$  for tank-treading vesicles, we obtain for  $\lambda = 1$

$$\Delta y_f - \Delta y_i = \frac{13R_0^3}{7\Delta y_i^2} \sqrt{\frac{5\Gamma}{6}} [1 - 4.526\Gamma + 29.16\Gamma^2 - 262.2\Gamma^3 + 2534.\Gamma^4 - 24640.\Gamma^5 + O(\Gamma^6)]. \quad (12)$$

Comparison between far-field analytical expansions and direct numerical simulations is shown in Fig. 4.

*Discussion.*—In order to evaluate the range of applicability of our analytical results [Eqs. (5) and (12)], we have performed direct numerical simulations of vesicle-vesicle and vesicle-wall interactions [28]. Figure 1 of Ref. [28] and Fig. 4 shows that long-range asymptotic laws [Eqs. (5) and (12)] interestingly capture the full numerical results quantitatively (within a few %) even for distances as small as two vesicle diameters.

The lift force due to vessel walls is a determinant factor in the microvasculature (capillaries, venules, and arterioles) as testified by the famous Fåhræus-Lindqvist effect [3] (drastic decrease of apparent blood viscosity when tube diameter decreases from about  $10^3$  to  $10 \mu\text{m}$ ). Furthermore, hematocrit in the microvasculature falls in the range 10–20% [23] where the semidilute regime makes sense. Another relevance of the lift force can be found in recent *in vitro* experiments [37] on separation of blood cells, which have been guided by an asymptotic theory on lift [9] of a single vesicle. Our result should provide a

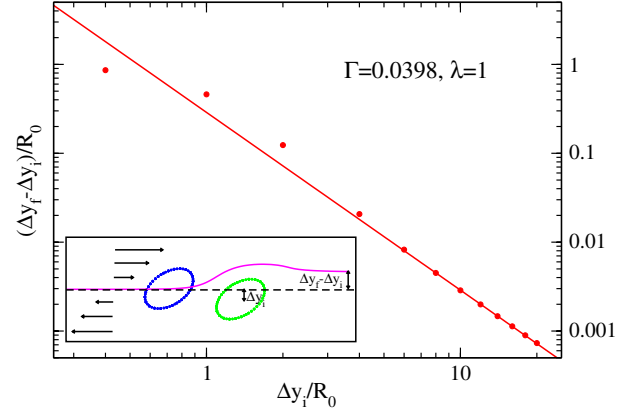


FIG. 4 (color online). Hydrodynamic interaction between two vesicles:  $\Delta y_f - \Delta y_i$  as a function of  $\Delta y_i$ . The solid line is calculated by Eq. (12), the symbols are results of full boundary integral simulations of two vesicles in shear flow with  $C_a = 100$ . The inset shows a schematic view of two vesicles interacting in shear flow as observed in the frame relative to one of the vesicles.

basis for further improvement of blood separation. Besides the wall lift force, we have found that in a Poiseuille flow the situation is quite complex, with a plethora of scenarios: migration away from center, or towards the center, and metastability, depending on flexibility and the flow strength. From this observation, we believe that this knowledge would advance rational design of the lab-on-chip technology. Additionally, the analytical study of hydrodynamic interaction opens the way to extract rather easily information on the hydrodynamic diffusion of semidilute suspensions. Interplay between lift due to wall and shear gradient and hydrodynamic diffusion is decisive for radial hematocrit distribution, that in turn, dictates the overall blood flow dissipation in the microvasculature. Finally, we hope that this work will incite new experiments on vesicles and RBCs in order to check the predictions, but also to draw similarities and dissimilarities between the two systems. This will constitute an essential piece of information in order to guide further theoretical development and especially, to better identify the role of the cytoskeleton in RBCs, the precise modeling of which is still matter for debate.

We would like to thank P.-Y. Gires, T. Podgorski, and P. M. Vlahovska for helpful discussions. We acknowledge financial support from CNES, ESA, and ANR (“MOSICOB” project).

\*alexandr.farutin@ujf-grenoble.fr

†chaouqi.misbah@ujf-grenoble.fr

[1] S. Wu, *Polym. Eng. Sci.* **19**, 638 (1979).

[2] R. H. Shafer, N. Laiken, and B. H. Zimm, *Biophys. Chem.* **2**, 180 (1974).

- [3] A. R. Pries, D. Neuhaus, and P. Gaetgens, *Am. J. Physiol.* **263**, H1770 (1992).
- [4] P. Vlahovska, T. Podgorski, and C. Misbah, *C.R. Physique* **10**, 775 (2009).
- [5] M. Abkarian, C. Lartigue, and A. Viallat, *Phys. Rev. Lett.* **88**, 068103 (2002).
- [6] G. Coupier, B. Kaoui, T. Podgorski, and C. Misbah, *Phys. Fluids* **20**, 111702 (2008).
- [7] V. Kantsler, E. Segre, and V. Steinberg, *Europhys. Lett.* **82**, 58 005 (2008).
- [8] N. Callens, C. Minetti, G. Coupier, M.-A. Mader, F. Dubois, C. Misbah, and T. Podgorski, *Europhys. Lett.* **83**, 24 002 (2008).
- [9] P. Olla, *J. Phys. II (France)* **7**, 1533 (1997).
- [10] P.M. Vlahovska and R. S. Gracia, *Phys. Rev. E* **75**, 016313 (2007).
- [11] U. Seifert, *Phys. Rev. Lett.* **83**, 876 (1999).
- [12] G. Danker, P.M. Vlahovska, and C. Misbah, *Phys. Rev. Lett.* **102**, 148102 (2009).
- [13] A. Farutin and C. Misbah, *Phys. Rev. E* **84**, 011902 (2011).
- [14] I. Cantat and C. Misbah, *Phys. Rev. Lett.* **83**, 880 (1999).
- [15] S. Sukumaran and U. Seifert, *Phys. Rev. E* **64**, 011916 (2001).
- [16] T. Secomb, B. Styp-Rekowska, and A. Pries, *Ann. Biomed. Eng.* **35**, 755 (2007).
- [17] B. Kaoui, G.H. Ristow, I. Cantat, C. Misbah, and W. Zimmermann, *Phys. Rev. E* **77**, 021903 (2008).
- [18] S. K. Doddi and P. Bagchi, *Int. J. Multiphase Flow* **34**, 966 (2008).
- [19] H. Zhao, A. P. Spann, and E. S. G. Shaqfeh, *Phys. Fluids* **23**, 121901 (2011).
- [20] B. Kaoui, A. Farutin, and C. Misbah, *Phys. Rev. E* **80**, 061905 (2009).
- [21] V. Kantsler and V. Steinberg, *Phys. Rev. Lett.* **95**, 258101 (2005).
- [22] M.-A. Mader, V. Vitkova, M. Abkarian, A. Viallat, and T. Podgorski, *Eur. Phys. J. E* **19**, 389 (2006).
- [23] Y. Fung, *Biomechanics* (Springer, New York, 1990).
- [24] G. K. Batchelor, *J. Fluid Mech.* **41**, 545 (1970).
- [25] U. Seifert, *Eur. Phys. J. B* **8**, 405 (1999).
- [26] D. Barthès-Biesel, *J. Fluid Mech.* **100**, 831 (1980).
- [27] A. Farutin, T. Biben, and C. Misbah, *Phys. Rev. E* **81**, 061904 (2010).
- [28] See Supplemental Material at <http://link.aps.org/supplemental/10.1103/PhysRevLett.110.108104> for description of analytical and numerical methods, full simulation of vesicle lift from a wall, analytical expansions without conversion of fractions, and high-resolution images of a vesicle in Poiseuille flow.
- [29] J.R. Smart and J.D.T. Leighton, *Phys. Fluids A* **3**, 21 (1991).
- [30] T. Biben, A. Farutin, and C. Misbah, *Phys. Rev. E* **83**, 031921 (2011).
- [31] G. Coupier, A. Farutin, C. Minetti, T. Podgorski, and C. Misbah, *Phys. Rev. Lett.* **108**, 178106 (2012).
- [32] R. Skalak and P.I. Branemark, *Science* **164**, 717 (1969).
- [33] T.W. Secomb and R. Skalak, *Microvasc. Res.* **24**, 194 (1982).
- [34] S. Guido and G. Tomaiuolo, *C.R. Physique* **10**, 752 (2009).
- [35] G. Tomaiuolo, M. Simeone, V. Martinelli, B. Rotoli, and S. Guido, *Soft Matter* **5**, 3736 (2009).
- [36] M. Abkarian, M. Faivre, R. Horton, K. Smistrup, C. A. Best-Popescu, and H. A. Stone, *Biomed. Mater.* **3**, 034011 (2008).
- [37] T.M. Geislinger, B. Eggart, S. Braunmüller, L. Schmid, and T. Franke, *Appl. Phys. Lett.* **100**, 183701 (2012).